https://doi.org/10.5194/egusphere-2024-881
Preprint. Discussion started: 3 April 2024

Future scenarios of albedo and radiative forcing resulting from changes in snow depth in Austria

Joseph Kiem[1,2], Albin Hammerle[1], Leonardo Montagnani[2], and Georg Wohlfahrt[1]

[1]University of Innsbruck, Innsbruck, Austria
[2]Free University of Bolzano, Bolzano/Bozen, Italy

Correspondence: Georg Wohlfahrt (Georg.Wohlfahrt@uibk.ac.at)

Abstract. The presence of a seasonal snowpack decisively modulates the albedo of terrestrial land surfaces. Global warming-driven decreases in the duration of the seasonal snow cover are thus expected to lower annual albedo, result in a positive radiative forcing and thus represent a positive feedback to climate change. Here we quantify future (up to the year 2100) scenarios of albedo change and the associated radiative forcing for Austria using a machine learning approach which leverages satellite-derived albedo data and future scenarios of snow depth. Albedo was calculated from the MODIS MCD43A1 v006 BRDF/albedo product for the period 2002-2019. Snow depth was taken from a novel dataset for Austria (FuSE-AT) covering the period 1951-2100. A machine-learning model (using LightGBM) was then trained to predict albedo separately for each land cover type (MODIS MCD12Q1 v006) using snow depth, days since last snowfall, as well as several predictors related to plant canopy structure (leaf area index, canopy height) and topography (latitude, longitude, elevation above sea level, inclination, exposition). LAI turned out to be an important predictor in simulating albedo in both snow free and snow covered points in time. Time since last snowfall, as a surrogate for snow aging, was more important for short land cover types than for forests. The correlation coefficients of the trained models varied widely across the different land cover types, ranging from 0.70 to 0.94. In 5 out of the 6 scenarios used, a significant decline of albedo could be observed. The cumulative time-dependent emission equivalent resulting from the albedo changes between 2020-2100 corresponds to 0.25-1 (RCP 2.6), 0.8-2.25 (RCP 4.5) or 1-5 (RCP 8.5) times the annual CO_2-equivalent emissions of Austria for the year 2021.

Keywords: machine learning, RCP, remote sensing, land cover, emission equivalents, climate model

1 Introduction

The fraction of the incoming solar energy reflected by the Earth back to space is referred to as the planetary albedo. Albedo is a fundamental component of the Earth's energy balance and processes that define or influence the albedo of Earth directly affect Earth's climate (Stephens et al., 2015). The Earth's planetary albedo is influenced by many factors, including cloud coverage, land cover, or snow and ice cover. Cloud cover influences albedo by modulating the amount of solar radiation reaching the Earth's surface and thus affecting the reflection of incoming sunlight. Land, snow, and ice cover influence albedo through their reflective properties and the amount of incoming solar radiation that they absorb or reflect.

https://doi.org/10.5194/egusphere-2024-881
Preprint. Discussion started: 3 April 2024

It is well known that the reflective nature of snow results in a higher albedo. Snow covered surfaces reflect a significant portion of the incoming solar radiation. Changes in snow conditions such as snow age, wetness, and pollutants can significantly influence surface albedo. Thus, the albedo of snow varies, ranging from 0.9 for fresh snow to about 0.4 for melting snow and can drop as low as 0.2 for contaminated snow (Hall and Martinec, 1985). As the climate undergoes unprecedented changes, alterations in temperature and precipitation patterns are affecting the duration, extent, and composition of snow cover across different landscapes. In recent years, snow cover shows a negative trend in a lot of regions (Notarnicola, 2020). A recent study shows a decreasing trend in March snowpack across the Northern Hemisphere from 1981 to 2020 (Gottlieb and Mankin, 2024).

While numerous studies have examined the impact of snow presence/absence on albedo, fewer have focussed on the influence of snow depth. This is significant since the amount of snow present can result in variations in albedo. Shorter vegetation may be entirely covered by even a small amount of snow, whereas forests might not be covered, the snow-free canopy elements thus lowering the ecosystem-scale albedo. For forests, maximum canopy height and the fraction of visible ground has been shown to be strongly correlated with albedo (Webster and Jonas, 2018). This variability of albedo response among land cover types underscores the significance of accounting for vegetation types when analyzing the influence of snow depth on albedo. Moreover, as previously mentioned, the aging of snow can play a crucial role, as it has the potential to significantly impact snow albedo.

Satellites have revolutionized our ability to observe our planet, providing a wealth of data that is now indispensable in climate science. This satellite-derived data offers a comprehensive and detailed perspective of the Earth's surface. The use of satellite-based observations enables the ongoing monitoring of these properties on a global scale. Liu et al. (2009) have already demonstrated the efficacy of satellite-derived data in accurately retrieving albedo. Data products derived from instruments such as the Moderate Resolution Imaging Spectroradiometer (MODIS) have proven instrumental in providing high-quality information at various spatial and temporal scales.

Comprehensively measuring snow depth at a high spatial resolution from ground observation systems presents substantial challenges. Additionally, gauging snow depth from space through satellites introduces its own set of difficulties. Hence, a large variety of approaches exists. Hedrick et al. (2015) used regional-scale lidar-derived measurements, Fernandes et al. (2018) measured snow depth changes using lightweight unmanned aerial vehicle videos and Daudt et al. (2023) used a neural network to estimate snow depth. Olefs et al. (2020) used a snow cover model together with simulated data from climate models to derive snow conditions. Here we used the snow data from Olefs et al. (2020) together with satellite-derived data products to train machine-learning models for each land cover type using data from 2002-2019.

Our primary objectives in this study are as follows:

1. Attempting to predict future albedo for Austria as influenced by changes in snow depth.
2. Quantifying the resulting radiative forcing due to albedo changes.
3. Demonstrating the significance of snow depth as a predictor in albedo modeling.
4. Highlighting the importance of snow aging (i.e. days since snowfall) as a predictor.

https://doi.org/10.5194/egusphere-2024-881
Preprint. Discussion started: 3 April 2024

2 Data & Methods

2.1 Study area

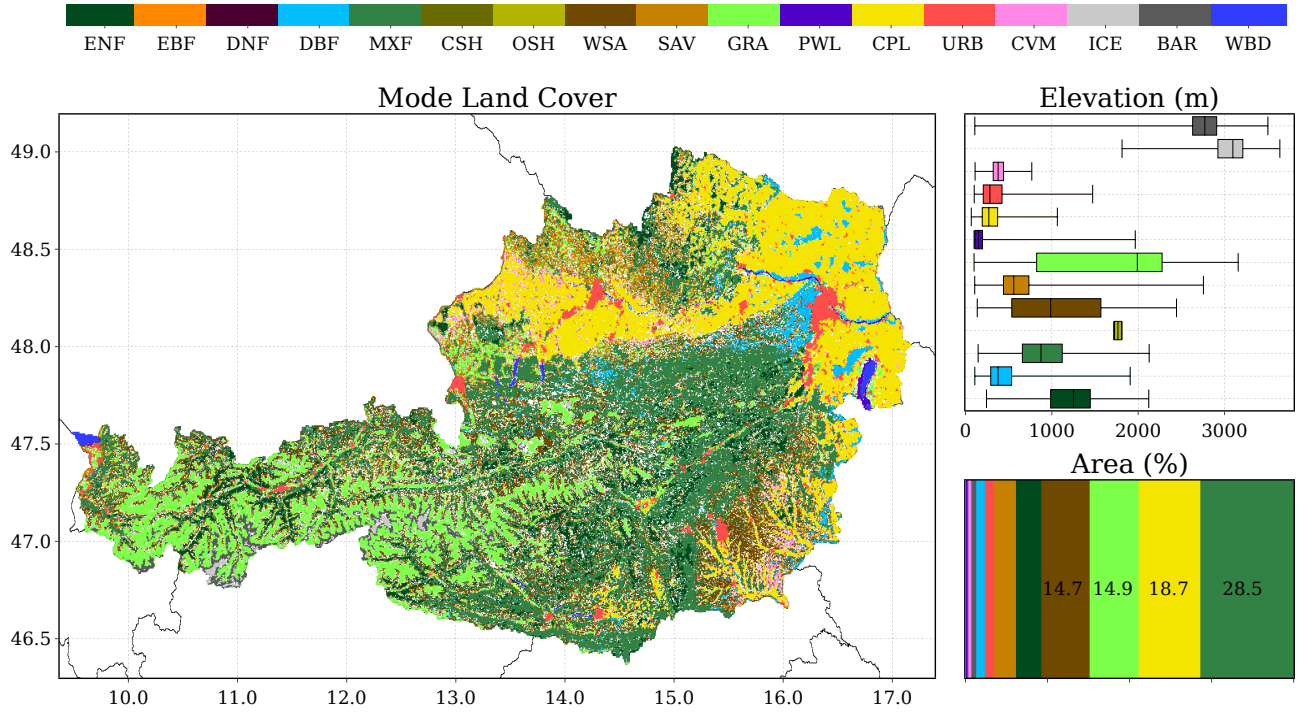

Figure 1. Land cover statistics: the mode of the land cover (MCD12Q1) of Austria from 2002 to 2019 (left). Elevation boxplots (upper right; only land cover types with enough data to compute statistics are displayed). Proportional area of each land cover type across the entire area (lower right). Definitions of abbreviations are summarized in Table A1.

Austria is a landlocked country in the Eastern Alps in Central Europe with an area of about 83,871 km^2. It lies between latitudes 46° and 49° N and longitudes 9° and 18° E (Figure 1). The minimum elevation above sea level in Austria is 112 meters, with a maximum elevation reaching 3795 meters (data from The Geoportal of the nine Austrian Provinces). Only 32% of the country is below 500 meters a.s.l. Austria lies in the temperate climate zone with an average temperature for the current reference period (1991 - 2020) of 7.4°C (data from GeoSphere Austria). The distribution of land cover types (MCD12Q1) of Austria are shown in Figure 1.

2.2 Snow depth data

The FuSE-AT (Olefs et al., 2020) snow depth (SD) data were downloaded at 1000m spatial resolution as NETCDF4 files. FuSE-AT provides daily modelled snow depth for Austria from 1951-2100. The data were upsampled to 500m spatial resolution and

https://doi.org/10.5194/egusphere-2024-881
Preprint. Discussion started: 3 April 2024

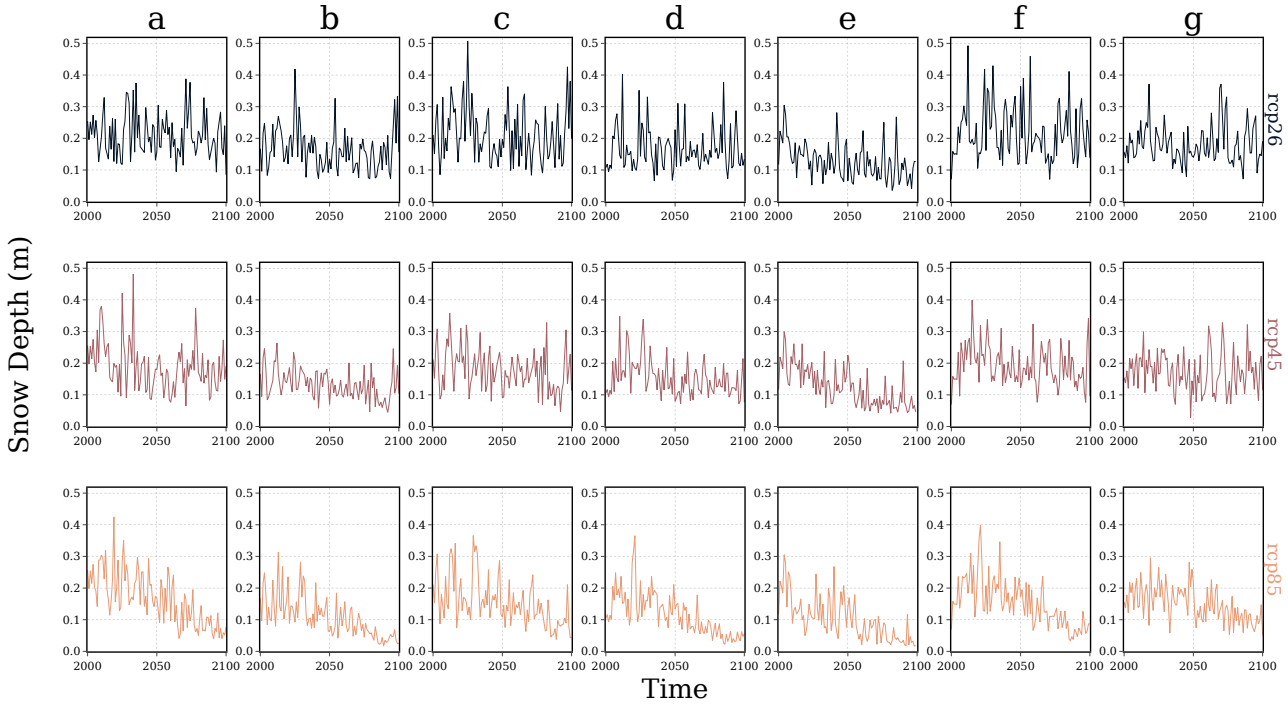

Figure 2. Yearly mean SD of Austria for the available FuSE-AT datasets (2000-2100). (a) MPI-M_MPI-ESM-LR_r2i1p1_MPI-CSC_REMO2009, (b) ICHEC_EC-EARTH_r12i1p1_SMHI_RCA4, (c) ICHEC_EC-EARTH_r12i1p1_CLMcom_CCLM4-8-17, (d) MPI-M_MPI-ESM-LR_r1i1p1_SMHI_RCA4, (e) MOHC_HadGEM2-ES_r1i1p1_SMHI_RCA4, (f) MPI-M_MPI-ESM-LR_r1i1p1_MPI-CSC_REMO2009, (g) ICHEC_EC-EARTH_r3i1p1_DMI_HIRHAM5.

reprojected to WGS84. Furthermore, these data were used to calculate days since last snowfall (DSS) and the border coordinates of FuSE-AT were used as the study area. The mask layer included in the FuSE-AT datasets was used to mask all the pixels outside of Austria.

Multiple FuSE-AT datasets are available based on different climate models (computer models to simulate the climate for a given time period) and ensembles (Figure 2). Each dataset is accessible in three versions, corresponding to one of the RCPs – specifically 2.6, 4.5, and 8.5, resulting in a total of 21 datasets. Due to computational overhead, only two of these were selected and used as inputs in this study. ICHEC_EC-EARTH_r12i1p1_CLMcom_CCLM4-8-17, based on the regional climate model COSMO-CLM from the Climate Limited-area Modelling Community (CLMcom) (Figure 2c) as one of the datasets with higher mean SD and MOHC_HadGEM2-ES_r1i1p1_SMHI_RCA4, based on the Rossby Centre regional atmospheric model RCA4 from the Hadley Centre Global Environment Model version 2 (HadGEM) (Figure 2e) as one of the datasets with lower mean SD. Based on CLMcom data (rcp26) for the current reference period (1991-2020), on average 3.1% of the Austria is covered by snow for at least 300 days annually, while 55.4% experiences snow cover for at least 100 days per year where the average

https://doi.org/10.5194/egusphere-2024-881
Preprint. Discussion started: 3 April 2024

snow cover duration for the whole country is 58.2 days. Comparatively, HadGem data (rcp26) indicate that on average 1.7% of Austria is covered by snow for at least 300 days annually, with 51.0% experiencing snow cover for at least 100 days annually during the same reference period where the average snow cover duration for the whole country is 53.7 days.

2.3 Remote sensing data

MODIS MCD43A1 v006 bidirectional reflectance distribution function (BRDF)/albedo model parameters (Schaaf and Wang, 2015), MCD12Q1 v006 land water mask and land cover product (Friedl and Sulla-Menashe, 2019), MCD15A3H v006 leaf area index/FPAR product (Myneni et al., 2015) at 500m spatial resolution and the ASTER digital elevation model v003 (NASA/METI/AIST/Japan Spacesystems And U.S./Japan ASTER Science Team, 2019) at 30m spatial resolution were downloaded as NETCDF4 files using the AppEEARS API (AppEEARS Team, 2023). The data were requested for the time period 2002-2019 using the bounding box created with the border coordinates of FuSE-AT. MCD12Q1 land cover data are available yearly, from which the mode was calculated for each pixel over the study period and used to represent land cover (Figure 1). Abbreviations were assigned to each land cover type (see Table A1). MCD15A3H leaf area index (LAI) data is available 4-daily. The missing days were linearly interpolated to obtain daily LAI. The ASTER digital elevation model was used to calculate aspect and slope.

The GEDI global forest canopy height 2019 (Potapov et al., 2021) was downloaded at 30m spatial resolution as a TIF file. It was cropped and downsampled to 500m spatial resolution to align it with the spatial extent of the rest of the data.

BESS global shortwave radiation data (Ryu et al., 2018) at 5000m resolution were downloaded as a NETCDF4 files. The data were cropped and upsampled to 500m spatial resolution. Together with the MODIS MCD43A1 BRDF parameters, actual (blue sky) albedo was then calculated following Wohlfahrt et al. (2021).

2.4 Machine learning model

In order to simulate albedo, the LightGBM model (Ke et al., 2017) was trained on the available data from 2002-2019. LightGBM showed the best trade-off in terms of memory consumption, prediction speed and prediction accuracy. Separate models were trained for each land cover type which were then joined to a "combined model" to predict future albedo, based on the different snow scenarios.

Besides SD, DSS turned out to be an important predictor in modelling albedo in preparatory analyses, since older snow tends to lower the albedo (Figure 3). All of the analysed land cover types showed this response with varying strengths, yet the most pronounced responses could be observed in lower statured land cover types. LAI depicted a similar pattern and proved to be important even at times when the ground was covered with snow (Figure 3). In addition to the already mentioned, canopy height, elevation, aspect, slope, latitude and longitude were included as predictors. Recursive feature elimination with cross-validation has been performed using the scikit-learn library (Pedregosa et al., 2011) which highlighted that every one of the selected predictors was important to simulate albedo. LightGBM parameters were optimized prior to training the models using a scikit-learn grid-search. During training, a validation dataset was used to prevent over-fitting using the L2-loss as a loss metric. 80% of the data were used for training, 10% for validation and 10% for testing. The training took approximately

https://doi.org/10.5194/egusphere-2024-881
Preprint. Discussion started: 3 April 2024

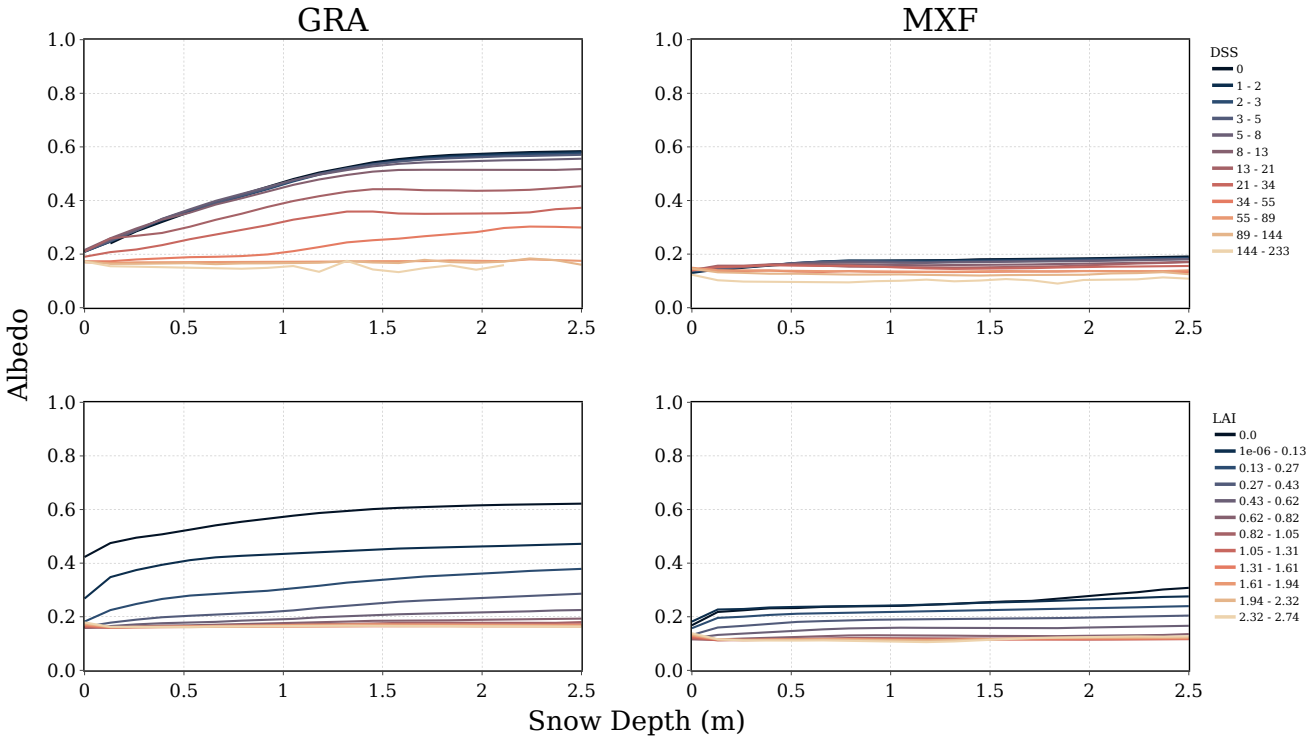

Figure 3. Mean albedo per SD of grasslands (left) and mixed forests (right) using all the available data from 2002-2019 (ICHEC_EC-EARTH_r12i1p1_CLMcom_CCLM4-8-17). Each line represents a different DSS (top) or LAI (bottom) class. The LAI-albedo-snow relationship for all land cover types is shown in Figure A1. Definitions of abbreviations are summarized in Table A1.

8 hours for a single snow scenario using 16 threads on an AMD Ryzen 7 processor. The model performance was evaluated using the test dataset, and multiple test metrics were computed; among others the Nash-Sutcliffe efficiency (NSE) (Nash and Sutcliffe, 1970) and the Kling-Gupta efficiency (KGE) (Gupta et al., 2009). The trained models were used to simulate daily albedo for the different snow scenarios from 2020 to 2100. This approach assumes that land cover type, the seasonal course of LAI (averaged over 2003-2019) and canopy height stay the same in the future and was trained on SD and DSS data from RCP 2.6 for both models.

2.5 Radiative forcing and time-dependent emission equivalent

The radiative forcing (W m^{-2}) due to albedo changes was calculated as:

$$\mathrm{RF}_{\Delta\alpha} = \frac{\sum_{m=1}^{12} K_m \Delta\alpha_m}{12} \frac{A_A}{A_E} \tag{1}$$

https://doi.org/10.5194/egusphere-2024-881
Preprint. Discussion started: 3 April 2024

where K_m is a monthly climatological albedo change radiative Kernel (W m^{-2}) (Bright and O'Halloran, 2019), $\Delta\alpha_m$ is the climatological monthly albedo difference between the average of the albedo of Austria from 2003-2032 and 2070-2099 and A_A and A_E are the surface areas (m^2) of Austria and the Earth respectively. Given the limited availability of LAI data, which commenced in July 2002, the year 2003 served as the starting point for the predictions in this study.

The time-dependent emission equivalent (kg $eCO_2 m^{-2} yr^{-1}$) was calculated following Bright et al. (2016) as:

$$\text{TDEE}_{\Delta\alpha} = {k_{CO_2}}^{-1} {Y_{CO_2}}^{-1} \text{RF}_{\Delta\alpha} \tag{2}$$

where ${k_{CO_2}}^{-1}$ is the radiative efficiency of CO_2 (1.76e-15 W $m^{-2} kg^{-1}$), ${Y_{CO_2}}^{-1}$ is the inverse of the lower triangular matrix used to solve the system of linear equations (Bright et al., 2016) and $\text{RF}_{\Delta\alpha}$ (Equation 1) was calculated using the monthly albedo difference between the reference time range (2003-2019) and the given year as $\Delta\alpha_m$. The atmospheric transmissivity and albedo change radiative kernels were calculated following Bright et al. (2020) using the EURO-CORDEX ensemble data (Jacob et al., 2013) on surface downwelling shortwave and top of the atmosphere incident shortwave radiation for the CLMcom and HadGEM scenarios, respectively. Based on the decision tree in Figure 2 of Bright and Lund (2021), the cumulative TDEE (e.g $\sum$ TDEE) is a solid choice in the context of this study. According to Bright et al. (2016), uncertainties associated with the TDEE largely stem from the uncertainty of the albedo model (or data).

2.6 Software

Data preparation, modelling and statistical analyses were carried out using Python 3.11 (Van Rossum and Drake, 2009). More time-intensive parts were written in the Rust programming language v1.73 (Matsakis and Klock II, 2014). Reprojections and cropping were carried out with the GDAL library (Rouault et al., 2023).

3 Results

Both combined calculated albedo models (CLMcom and HadGEM) show a similar performance (Figure 4a and Figure A2a). Since the combined models were composed of sub-models for each land cover type, their skill could be determined separately (Table A2). Open shrublands (NSE 0.89, KGE 0.94) and grasslands (NSE 0.82, KGE 0.86) together with some of the other shorter vegetation types showed the best performance. In the case of forest types and croplands, a lower model performance was observed. Deciduous broadleaf forests (NSE 0.59, KGE 0.66) displayed the highest and deciduous needleleaf forests (NSE 0.53, KGE 0.52) together with evergreen needleleaf forests (NSE 0.49, KGE 0.56) the lowest test metrics among the forest types. The combined albedo models generally showed a positive bias of predictions (Figure 4b and Figure A2b). Due to the non-linear response of albedo to LAI during periods of snow cover (Figure 3), the usage of average seasonal LAI as an input to the albedo model resulted in an underestimation of albedo, especially in winter, for certain land cover types (Figure A3 and Figure A4).

https://doi.org/10.5194/egusphere-2024-881
Preprint. Discussion started: 3 April 2024

Among the sub-models, deciduous needleleaf forests and open shrublands showed the highest bias and urban and permanent wetlands the lowest (Table A2). For croplands, an exploratory analysis revealed that the model skill could be increased by further subdividing them into more specific subclasses such as pastures, vineyards, and farmland, based on CORINE land cover classes (European Environment Agency, 2019) (data not shown).

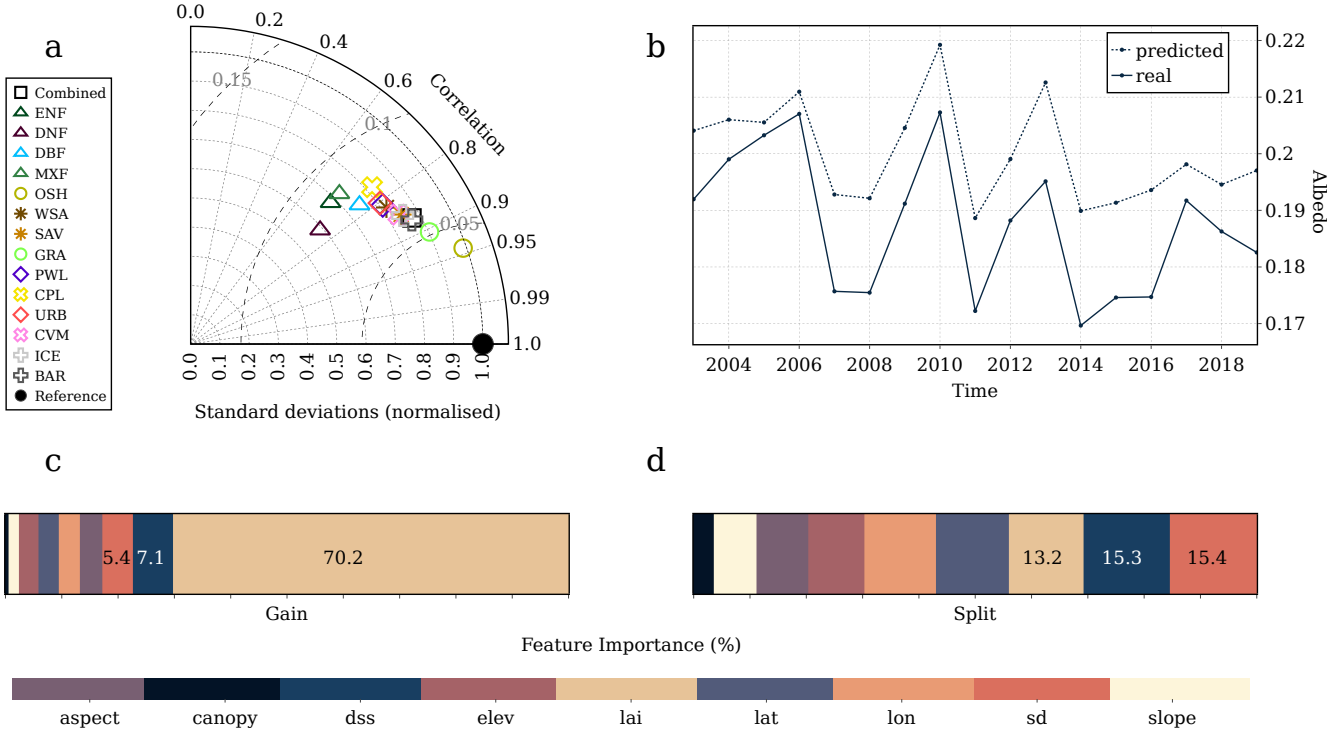

Figure 4. Model statistics: (a) Taylor diagram for the combined model and its sub-models. Standard deviations (radial axis) are normalised to the reference standard deviation. (b) Yearly mean predicted (dashed line) vs. actual (solid line) albedo (2003-2019). (c) Combined gain feature importance of all sub-models. (d) Combined split feature importance of all submodels. Since both models (CLMcom and HadGEM) display very similar statistics, only CLMcom is shown here. Definitions of abbreviations are summarized in Table A1.

The combined feature importance for the two calculated albedo models are shown in Figure 4c and d and Figure A2 c and d. LAI displayed a very high gain feature importance (70.2% CLMcom, 69.9% HadGEM) in all land cover types, meaning LAI attributed a lot to the information gain. SD (15.4% CLMcom, 15.0% HadGEM) and DSS (15.3% CLMcom, 15.8% HadGEM) were among the highest in split feature importance, meaning they were used more frequently for splitting (making decisions) in the model. This was also true for a model which excludes instants in time when SD equals 0. LAI maintained a high gain feature importance of 68.0%, while SD (21.0%) and DSS (11.3 %) were still at the top of the split feature importance, which means LAI was important to model the albedo for snow covered and not snow covered points in time, confirming the results of the exploratory analysis shown in Figure 3.

https://doi.org/10.5194/egusphere-2024-881
Preprint. Discussion started: 3 April 2024

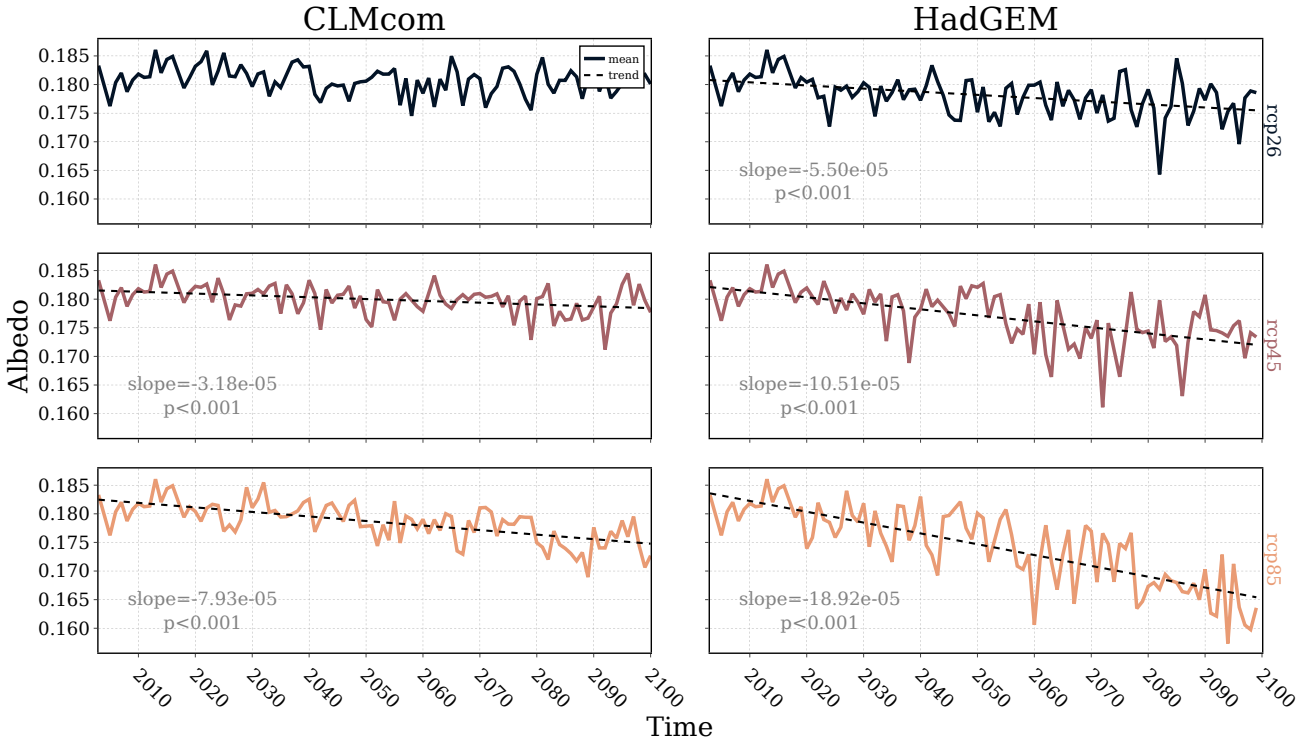

Figure 5. Yearly mean simulated albedo 2003-2100 of Austria for the three different scenarios for both models. The dashed line represents a linear regression over the mean values and is shown when the slope is significantly different from zero ($\alpha = 0.05$).

Yearly averages showed a significant decline of albedo over the years for the RCP 4.5 and RCP 8.5 scenarios (Figure 5). This was true for both CLMcom and HadGEM, while HadGEM also showed a significant decline for the RCP 2.6 scenario and stronger declines for RCP 4.5 and RCP 8.5.

The radiative forcing resulting from albedo changes showed the lowest values for the RCP 2.6 scenario and the highest for the RCP 8.5 scenario in both CLMcom and HadGEM, as indicated in Table A3. HadGEM consistently displayed higher values than CLMcom, due to the greater decrease in albedo. The cumulative time-dependent emission equivalents for the RCP 2.6, 4.5, and 8.5 scenarios were 14.5, 40.7, and 118.0 Mt CO_2 for CLMcom, and 50.1, 115.4, and 260.3 Mt CO_2 for HadGEM, respectively (Figure 6). HadGEM consistently demonstrated higher values than CLMcom across the scenarios, mirroring the observed trends in radiative forcing from albedo changes (Table A3).

4 Discussion

The results of the machine learning-based simulations present an insight into possible future dynamics of albedo, driven primarily by changes in snow depth and time since last snowfall under the RCP 2.6, 4.5 and 8.5 scenarios. The simulations

https://doi.org/10.5194/egusphere-2024-881
Preprint. Discussion started: 3 April 2024

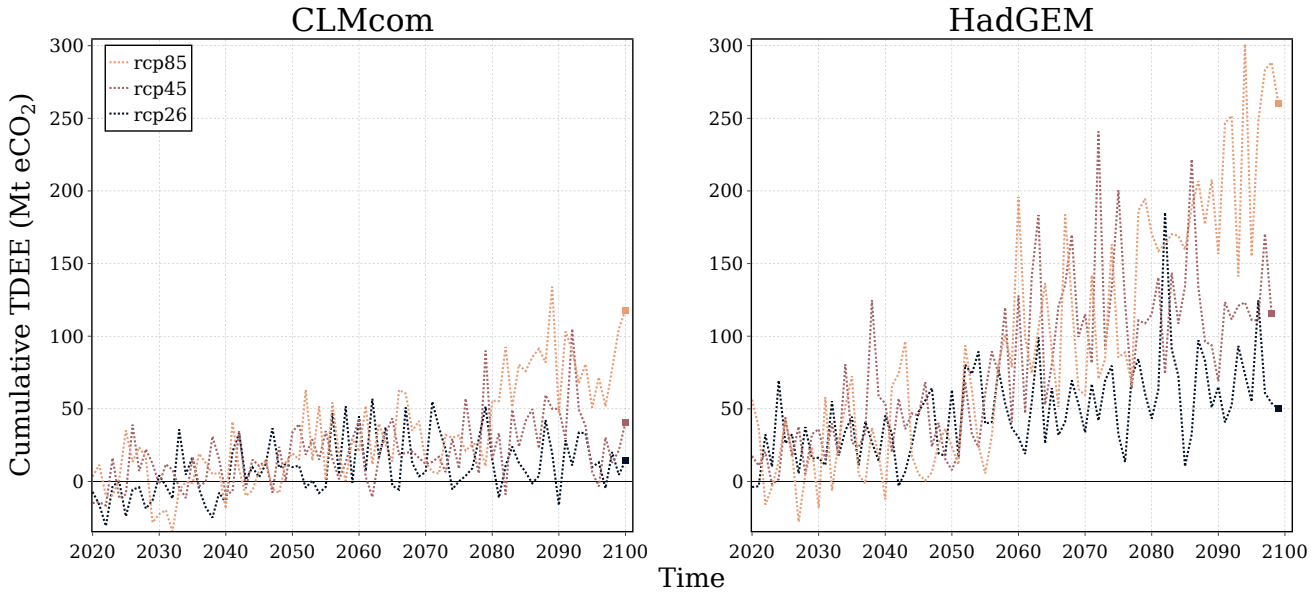

Figure 6. Cumulative sum of the time-dependent emission equivalent of Austria for the two selected snow scenarios.

indicate negative trends in albedo, particularly in the RCP 4.5 and 8.5 scenarios. Moreover, the extent of albedo change is significantly influenced by the choice of climate model used in generating snow depth products. Here we intentionally selected two climate models that differ greatly in terms of future SD development, which resulted in inter-model albedo differences to exceed differences between RCPs of the single models.

Exploratory analysis showed correlations among DSS, SD, LAI and albedo (Figure 3). These correlations were especially evident in shorter vegetation types. Fresh snow typically possesses a naturally high albedo, but this reflectivity can diminish over time, for instance, through processes like contamination by various pollutants or increasing water content (Wiscombe and Warren, 1980; Chen et al., 2014). Furthermore, the albedo is dependent on the canopy and the bare soil that it is going to shade (Lugato et al., 2020). Forests usually have a very low albedo due to their high canopy density and and their ability to mask the high albedo of snow on the ground or in the understory (Bonan, 2008). The albedo of forests also generally increases less with snow while the albedos of nonforested surfaces become much larger with snow (Jin et al., 2002).

The test runs for the trained sub-models revealed that not every land cover type is easily modelled (Figure 4a). Figure A3 and Figure A4 illustrate a notable discrepancy between predicted and modeled albedo, particularly during winter months, for forest land cover types and croplands. The utilization of seasonal mean LAI appears to distort albedo values in winter, highlighting the significance of considering LAI during this season for accurate albedo simulation. Even when incorporating actual LAI values, there remains a slight deviation in albedo for the specified land cover types, indicating the possible necessity for additional predictors. Another explanation could be that the seasonal mean LAI does not accurately reflect the albedo. The mean albedo is influenced in a non-linear fashion by a few instances of high albedo with low LAI and numerous instances of low albedo

https://doi.org/10.5194/egusphere-2024-881
Preprint. Discussion started: 3 April 2024

with high LAI (Figure 3, Figure A1). Using the mean LAI would therefore result in a lower albedo than the true mean. It seems plausible that land cover types with a low LAI dependency would exhibit reduced seasonal bias when using the mean LAI.

LAI was shown to be a crucial predictor in the albedo simulation. Bsaibes et al. (2009) investigated the LAI-albedo relationship for croplands and concluded that it is influenced by multiple factors such as soil background, canopy architecture, and potentially other variables like chlorophyll content. In the context of this study, comprehending the LAI-albedo relationship might pose additional challenges, given the investigation of multiple land cover types.

The predicted albedo allowed us to calculate the radiative forcing due to albedo changes, which is however unfamiliar to many and hard to put into perspective. We thus followed Bright et al. (2016) and calculated cumulative time-dependent emissions equivalence metrics, which yields the accumulated CO_2-equivalent emissions that these positive radiative forcings correspond to. The quantification of the emission-equivalents underscores the significance of the albedo decrease. Even though the predicted changes in albedo may appear small (Figure 5), the resulting albedo changes can have a huge impact on Earth's climate, which has been known for a long time. Sagan et al. (1979) already discussed how alterations in land cover, such as deforestation and urbanization, can influence albedo and subsequently contribute to changes in the Earth's climate. The significance of albedo changes may not be immediately apparent, but their emission-equivalents cumulate to years worth of greenhouse gas emissions. In 2021, Austria emitted 48.8 Mt of CO_2 equivalents (Umweltbundesamt GmbH, 2023), covered by the EU Regulation 2018/842 (European Parliament and Council, 2018). The predicted cumulative TDEE (Figure 6) thus corresponds to 0.25-1 (RCP 2.6), 0.8-2.25 (RCP 4.5) or 1-5 (RCP 8.5) times the annual CO_2-equivalent emissions of Austria for the year 2021.

A limitation of the model lies in its assumption of constant future parameters, namely LAI, land cover, and canopy height. Changes in these factors over time, such as alterations in land cover due to abandonment or shifts in vegetation patterns resulting from global warming or bio-based climate mitigation efforts, are not accounted for. The susceptibility to land abandonment in mountainous regions, like Austria, is particularly pronounced (Dax et al., 2021). Climate warming can exacerbate the frequency and severity of drought events, reducing soil moisture availability and increasing water stress on vegetation. Such conditions can lead to significant vegetation change and decreased vegetation coverage over time (Yin et al., 2023). Furthermore, research by Ridgwell et al. (2009) highlights that bio-geoengineering techniques, particularly those focused on leaf albedo modification, can induce dynamic alterations in vegetation properties and, consequently, surface albedo. All of these factors could significantly impact surface albedo, potentially leading to discrepancies between model predictions and real-world observations. Therefore, the model's ability to accurately capture long-term trends and dynamics may be limited by the static representation of these key variables.

The observed decrease in albedo carries substantial implications for the energy balance of Austria and national efforts towards reaching climate neutrality. Although snow cover (presence/absence) may be the predominant factor influencing albedo changes in the future, it is essential to acknowledge the role of snow depth in accurately modeling albedo. It has been shown, that a certain snow depth is necessary to effectively mask the underlying surface (Baker et al., 1991). Our study reveals that particularly for shorter vegetation, the combination of average snow depth and snow aging (DSS) contributes substantially to observed variability in albedo during snow-covered conditions (Figure 3). Incorporating these factors into climate models

https://doi.org/10.5194/egusphere-2024-881
Preprint. Discussion started: 3 April 2024

might be essential for ensuring accurate representations of albedo dynamics in seasonally snow-covered regions in response to changing environmental conditions. Such refinements contribute to a more comprehensive understanding of the complex interplay between canopy and snow characteristics in governing albedo, crucial for reliable climate predictions.

Code availability. The Python and Rust code used to analyse the data are freely available at https://doi.org/10.5281/zenodo.10907185.

Data availability. The data used in this analysis are freely available from the following sources: FuSE-AT: https://data.ccca.ac.at; BESS: http://environment.snu.ac.kr/bess_rad/; GEDI: https://glad.umd.edu/dataset/gedi; MODIS and ASTER: https://appeears.earthdatacloud.nasa.gov/; CACK: https://doi.org/10.6073/pasta/d77b84b11be99ed4d5376d77fe0043d8; EURO-CORDEX: https://www.euro-cordex.net/.

Author contributions. JK conceived the study in close collaboration with GW and AH. JK wrote the manuscript with the help of GW, AH and LM.

Competing interests. The authors declare no competing interests.

Acknowledgements. I thank GW and AH for proposing the topic of this study and providing valuable information during the analysis and GW, AH, and LM for their support and feedback during the writing of this article. The authors acknowledge Geosphere Austria for making the FuSE-AT dataset, which was funded within the frame of the 10th ACRP call (project number KR17AC0K13673), available.

https://doi.org/10.5194/egusphere-2024-881
Preprint. Discussion started: 3 April 2024

Appendix A: Tables

Table A1. MODIS land cover names and selected abbreviations.

Original name	Abbreviation
Barren	BAR
Closed Shrublands	CSH
Cropland Natural Vegetation Mosaics	CVM
Croplands	CPL
Deciduous Broadleaf Forests	DBF
Deciduous Needleleaf Forests	DNF
Evergreen Broadleaf Forests	EBF
Evergreen Needleleaf Forests	ENF
Grasslands	GRA
Mixed Forests	MXF
Open Shrublands	OSH
Permanent Snow and Ice	ICE
Permanent Wetlands	PWL
Savannas	SAV
Urban and Built up Lands	URB
Water Bodies	WBD
Woody Savannas	WSA

Table A2. Metrics calculated against the test dataset: bias = overall bias, corr = Pearson correlation coefficient, crmsd = centered pattern root mean square deviation, kge = Kling-Gupta efficiency, mae = mean absolute prediction error, me = mean prediction error, mse = mean squared error, nse = Nash-Sutcliffe efficiency, r2 = coefficient of determination, rmse = root mean squared error, sde = standard deviation of the error, std = standard deviation. Definitions of abbreviations are summarized in Table A1.

ICHEC_EC-EARTH_r12i1p1_CLMcom_CCLM4-8-17

	ALL	BAR	CPL	CVM	DBF	DNF	ENF	GRA	ICE	MXF	OSH	PWL	SAV	URB	WSA
bias	0.00054	0.00007	-0.00023	-0.00002	-0.00001	0.00435	0.00001	0.00002	-0.00061	-0.00070	-0.00559	0.00000	-0.00001	-0.00000	-0.00018
corr	0.86877	0.87207	0.75637	0.84872	0.77173	0.75049	0.70341	0.90521	0.85498	0.70336	0.94321	0.81074	0.85164	0.80192	0.82010
crmsd	0.05979	0.11770	0.06696	0.04863	0.03415	0.04644	0.04161	0.08538	0.09436	0.04680	0.08972	0.03110	0.05598	0.04117	0.06371
kge	0.81643	0.81607	0.69747	0.77801	0.66044	0.51954	0.56418	0.86430	0.79032	0.59446	0.94094	0.73230	0.78596	0.72389	0.74331
mae	0.03467	0.08511	0.03581	0.02716	0.02169	0.02693	0.02710	0.05174	0.07048	0.03003	0.05667	0.02083	0.03223	0.02338	0.03789
me	0.00054	0.00007	-0.00023	-0.00002	-0.00001	0.00435	0.00001	0.00002	-0.00061	-0.00070	-0.00559	0.00000	-0.00001	-0.00000	-0.00018
mse	0.00358	0.01385	0.00448	0.00236	0.00117	0.00218	0.00173	0.00729	0.00890	0.00219	0.00808	0.00097	0.00313	0.00169	0.00406
nse	0.75474	0.76048	0.56796	0.72020	0.59503	0.53349	0.49427	0.81940	0.73094	0.49419	0.88716	0.65730	0.72526	0.64304	0.67255
r2	0.75474	0.76048	0.56796	0.72020	0.59503	0.53349	0.49427	0.81940	0.73094	0.49419	0.88716	0.65730	0.72526	0.64304	0.67255
rmse	0.05980	0.11770	0.06696	0.04863	0.03415	0.04665	0.04161	0.08538	0.09436	0.04681	0.08989	0.03110	0.05598	0.04117	0.06372
sde	0.05979	0.11770	0.06696	0.04863	0.03415	0.04644	0.04161	0.08538	0.09436	0.04680	0.08972	0.03110	0.05598	0.04117	0.06371
std	0.10525	0.20871	0.08361	0.07699	0.04017	0.04031	0.03982	0.18139	0.15437	0.04762	0.26452	0.04307	0.09033	0.05565	0.09096

MOHC_HadGEM2-ES_r1i1p1_SMHI_RCA4

	ALL	BAR	CPL	CVM	DBF	DNF	ENF	GRA	ICE	MXF	OSH	PWL	SAV	URB	WSA
bias	0.00079	0.00003	0.00015	-0.00002	-0.00001	0.00241	0.00005	-0.00015	-0.00064	-0.00048	-0.00352	0.00002	0.00008	0.00002	-0.00014
corr	0.87349	0.88282	0.75853	0.84543	0.77818	0.71252	0.70819	0.90721	0.85380	0.71162	0.94930	0.81257	0.85206	0.79343	0.82334
crmsd	0.05878	0.11297	0.06669	0.04911	0.03372	0.04803	0.04133	0.08452	0.09472	0.04625	0.08473	0.03097	0.05591	0.04194	0.06320
kge	0.81958	0.83043	0.69929	0.77438	0.67101	0.62563	0.57108	0.86653	0.80002	0.60466	0.94717	0.73376	0.78576	0.71358	0.74661
mae	0.03413	0.08199	0.03548	0.02726	0.02137	0.02673	0.02683	0.05125	0.06944	0.02958	0.05450	0.02060	0.03215	0.02353	0.03757
me	0.00079	0.00003	0.00015	-0.00002	-0.00001	0.00241	0.00005	-0.00015	-0.00064	-0.00048	-0.00352	0.00002	0.00008	0.00002	-0.00014
mse	0.00346	0.01276	0.00445	0.00241	0.00114	0.00231	0.00171	0.00714	0.00897	0.00214	0.00719	0.00096	0.00313	0.00176	0.00399
nse	0.76295	0.77935	0.57149	0.71466	0.60512	0.50412	0.50103	0.82302	0.72887	0.50603	0.89958	0.66026	0.72596	0.62946	0.67786
r2	0.76295	0.77935	0.57149	0.71466	0.60512	0.50412	0.50103	0.82302	0.72887	0.50603	0.89958	0.66026	0.72596	0.62946	0.67786
rmse	0.05879	0.11297	0.06669	0.04911	0.03372	0.04809	0.04133	0.08452	0.09472	0.04626	0.08480	0.03097	0.05591	0.04194	0.06320
sde	0.05878	0.11297	0.06669	0.04911	0.03372	0.04803	0.04133	0.08452	0.09472	0.04625	0.08473	0.03097	0.05591	0.04194	0.06320
std	0.10522	0.21101	0.08362	0.07682	0.04062	0.05195	0.04012	0.18163	0.15710	0.04802	0.26412	0.04308	0.09025	0.05523	0.09112

https://doi.org/10.5194/egusphere-2024-881
Preprint. Discussion started: 3 April 2024

Table A3. Radiative forcing (μW m^{-2}) calculated from the monthly albedo difference between the average of the albedo of Austria from 2003-2032 and 2070-2099 (sorted from highest to lowest). The sum of separate land cover values does not equal ALL since we use the area of Austria, ignoring that not all pixels are classified (unclassified land cover). Furthermore, the area of the separate land covers was estimated using the number of pixels for a certain land cover type multiplied by the ratio of the area of Austria to the total sum of pixels inside Austria. Definitions of abbreviations are summarized in Table A1.

ICHEC_EC-EARTH_r12i1p1_CLMcom_CCLM4-8-17

	ALL	GRA	WSA	MXF	BAR	ENF	SAV	ICE	CPL	DBF	CVM	PWL	URB	OSH	DNF
rcp26	19.43	6.10	3.43	2.38	1.03	0.87	1.08	0.28	1.34	0.04	0.15	0.01	0.12	0.00	0.00
rcp45	28.35	9.37	4.89	4.90	2.32	1.52	1.07	0.31	0.15	0.25	0.07	0.02	0.04	0.00	0.00
rcp85	65.99	24.16	11.14	10.07	5.29	3.42	2.57	0.86	-0.64	0.45	0.17	0.07	-0.10	0.00	0.00

MOHC_HadGEM2-ES_r1i1p1_SMHI_RCA4

	ALL	GRA	MXF	WSA	CPL	ENF	BAR	SAV	URB	DBF	ICE	CVM	PWL	OSH	DNF
rcp26	50.16	14.49	9.02	8.85	2.85	2.61	2.67	1.60	0.40	0.27	0.49	0.09	0.03	0.00	0.00
rcp45	115.47	32.79	20.09	20.44	7.24	6.69	6.03	3.26	1.51	0.84	1.05	0.17	0.17	0.00	0.00
rcp85	260.31	59.42	55.67	38.09	27.50	13.52	8.58	8.73	9.01	4.32	1.10	0.95	0.82	0.00	0.00

https://doi.org/10.5194/egusphere-2024-881
Preprint. Discussion started: 3 April 2024

Appendix B: Figures

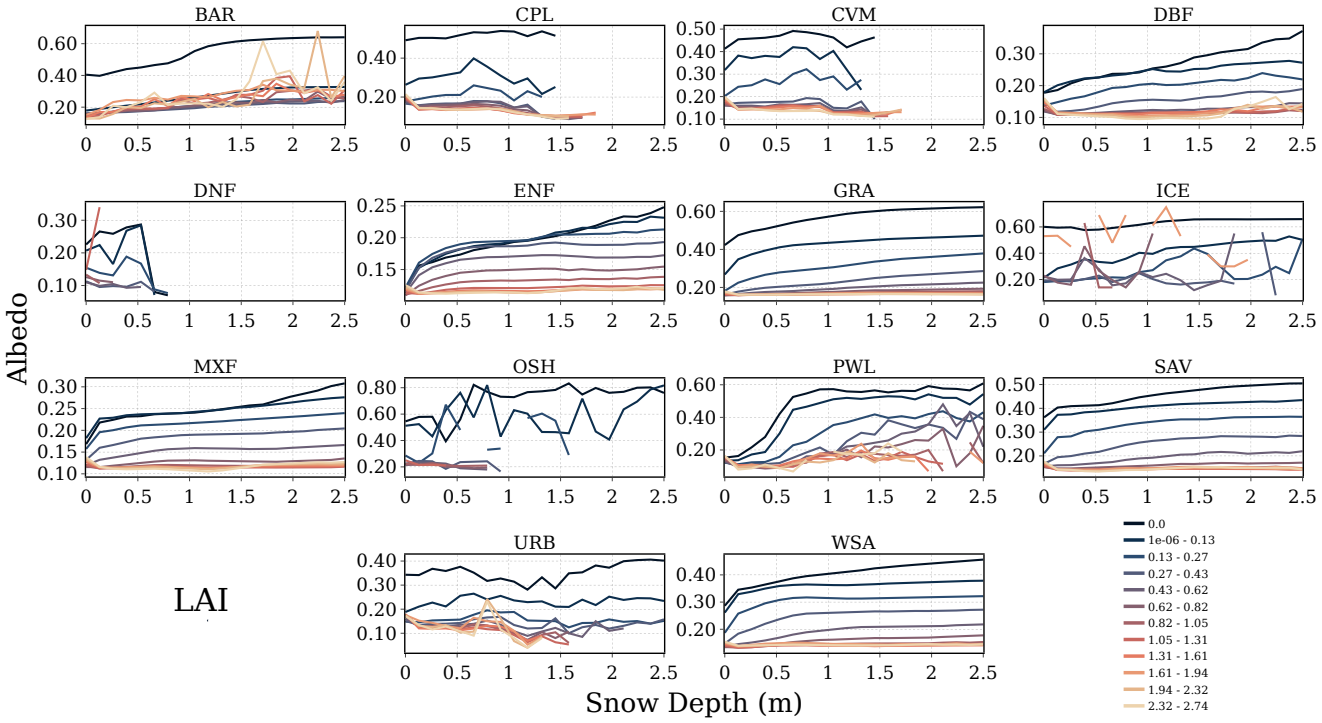

Figure A1. Mean albedo per SD using all the available data from 2002-2019 (ICHEC_EC-EARTH_r12i1p1_CLMcom_CCLM4-8-17). Each line represents a different LAI class. Note the different y-axis limits on the various panels. Definitions of abbreviations are summarized in Table A1.

https://doi.org/10.5194/egusphere-2024-881
Preprint. Discussion started: 3 April 2024

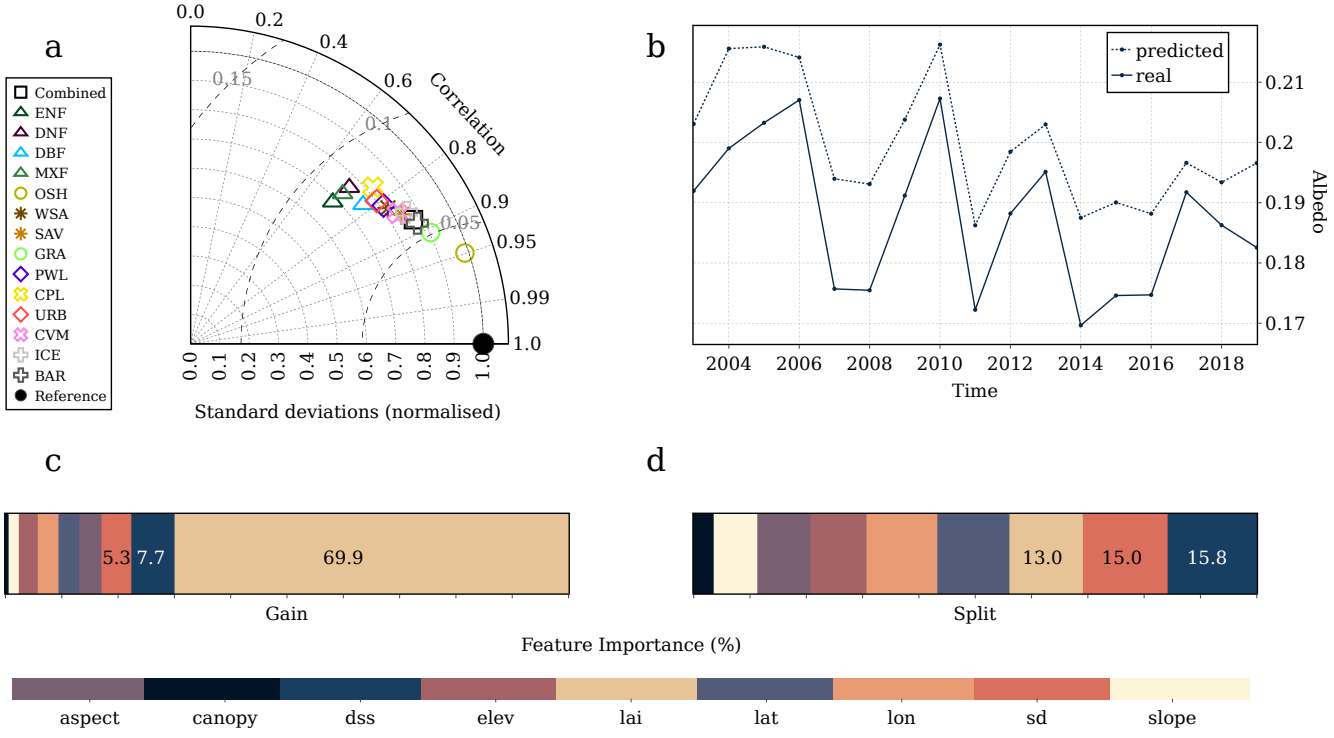

Figure A2. Model statistics MOHC_HadGEM2-ES_r1i1p1_SMHI_RCA4: (a) Taylor diagram for the combined model and its sub-models. Standard deviations (radial axis) are normalised to the reference standard deviation. (b) Yearly mean predicted (dashed line) vs. actual (solid line) albedo (2003-2019). (c) Combined gain feature importance of all sub-models. (d) Combined split feature importance of all submodels. Definitions of abbreviations are summarized in Table A1.

https://doi.org/10.5194/egusphere-2024-881
Preprint. Discussion started: 3 April 2024

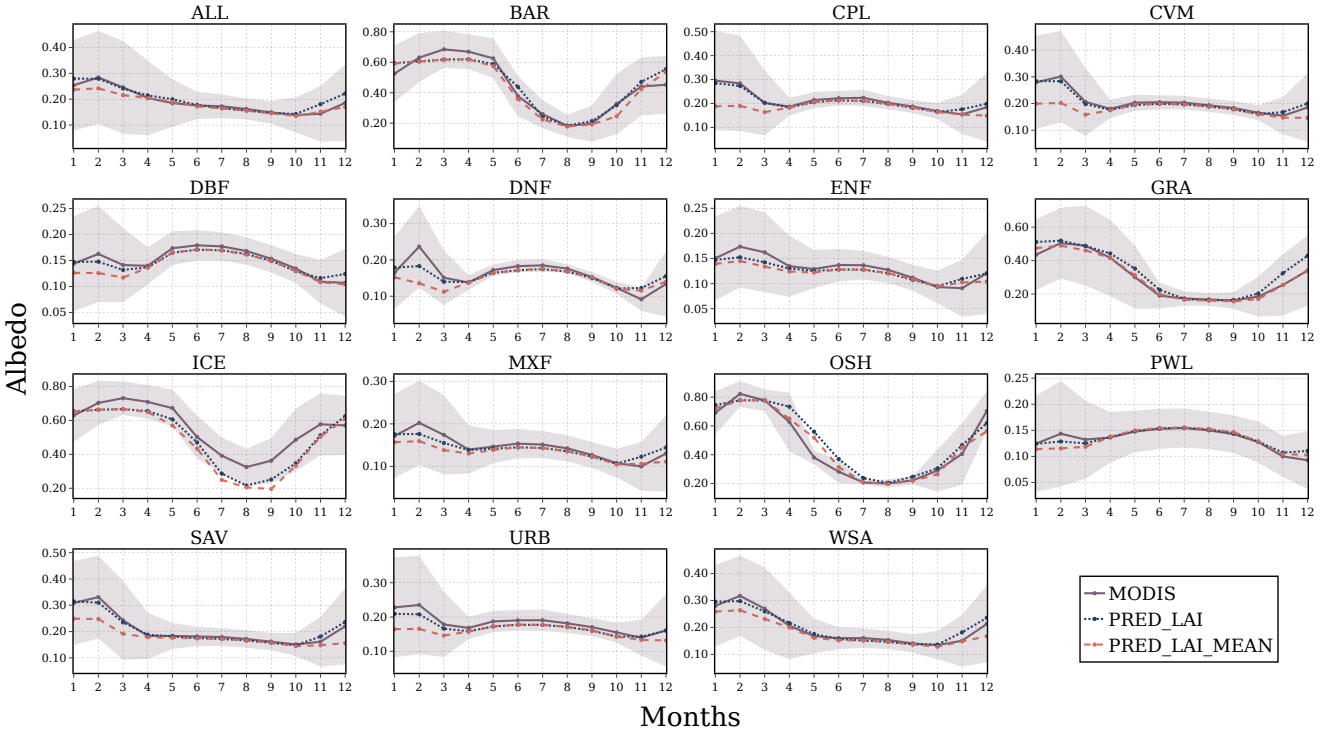

Figure A3. Mean albedo per month (2003-2019) for ICHEC_EC-EARTH_r12i1p1_CLMcom_CCLM4-8-17: the solid line (MODIS) shows the actual albedo. The dotted blue line (PRED_LAI) shows the predicted albedo using the actual LAI data. The dashed line (PRED_LAI_MEAN) shows the predicted albedo using seasonal LAI (averaged over 2003-2019). The shaded area shows the standard deviation of the actual (MODIS) albedo. Note the different y-axis limits on the various panels. Definitions of abbreviations are summarized in Table A1.

https://doi.org/10.5194/egusphere-2024-881
Preprint. Discussion started: 3 April 2024

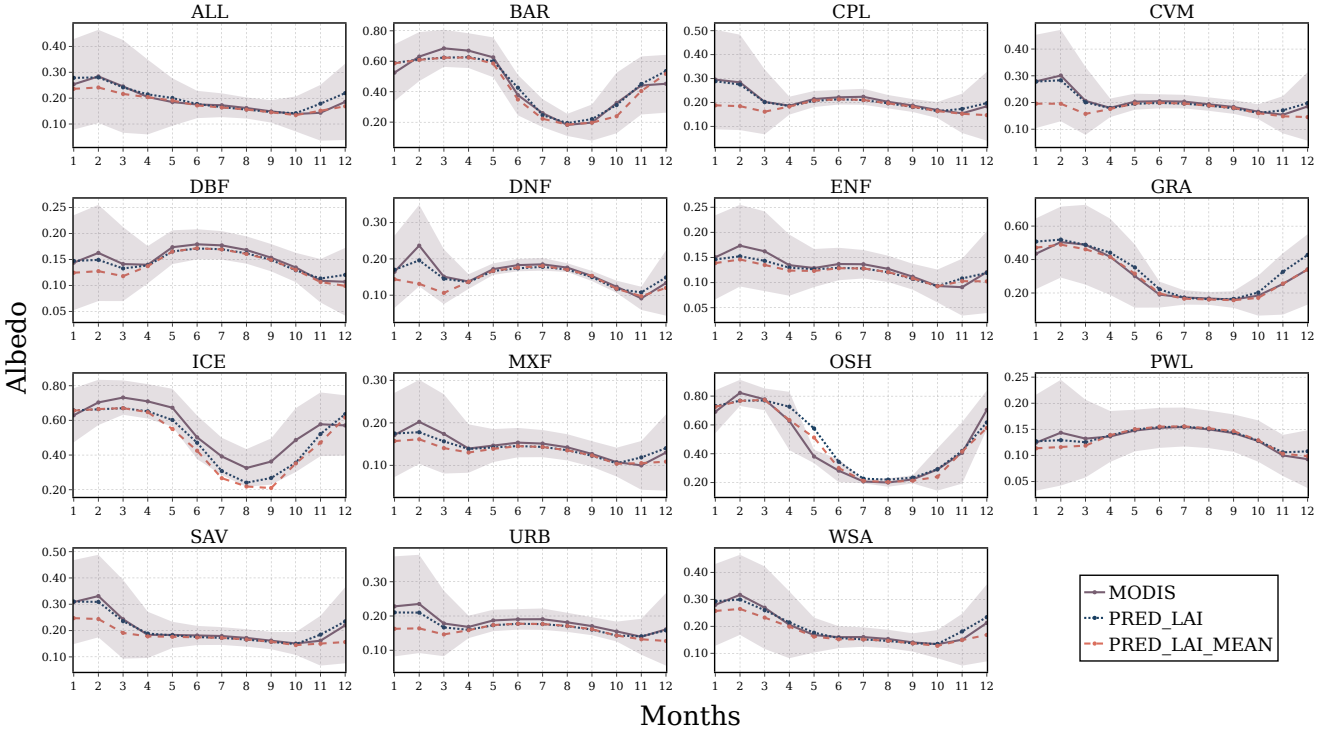

Figure A4. Mean albedo per month (2003-2019) for MOHC_HadGEM2-ES_r1i1p1_SMHI_RCA4: the solid line (MODIS) shows the actual albedo. The dotted blue line (PRED_LAI) shows the predicted albedo using the actual LAI data. The dashed line (PRED_LAI_MEAN) shows the predicted albedo using seasonal LAI (averaged over 2003-2019). The shaded area shows the standard deviation of the actual (MODIS) albedo. Note the different y-axis limits on the various panels. Definitions of abbreviations are summarized in Table A1.

https://doi.org/10.5194/egusphere-2024-881
Preprint. Discussion started: 3 April 2024

References

AppEEARS Team: Application for Extracting and Exploring Analysis Ready Samples (AppEEARS). Ver. 3.6, https://appeears.earthdatacloud.nasa.gov, 2023.

Baker, D. G., Skaggs, R. H., and Ruschy, D. L.: Snow Depth Required to Mask the Underlying Surface, Journal of Applied Meteorology, 30, 387–392, https://doi.org/10.1175/1520-0450(1991)030<0387:sdrtmt>2.0.co;2, 1991.

Bonan, G. B.: Forests and Climate Change: Forcings, Feedbacks, and the Climate Benefits of Forests, Science, 320, 1444–1449, https://doi.org/10.1126/science.1155121, 2008.

Bright, R. M. and Lund, M. T.: CO_2-equivalence metrics for surface albedo change based on the radiative forcing concept: a critical review, Atmospheric Chemistry and Physics, 21, 9887–9907, https://doi.org/10.5194/acp-21-9887-2021, 2021.

Bright, R. M. and O'Halloran, T. L.: Developing a monthly radiative kernel for surface albedo change from satellite climatologies of Earth's shortwave radiation budget: CACK v1.0, Geoscientific Model Development, 12, 3975–3990, https://doi.org/10.5194/gmd-12-3975-2019, 2019.

Bright, R. M., Bogren, W., Bernier, P., and Astrup, R.: Carbon-equivalent metrics for albedo changes in land management contexts: relevance of the time dimension, Ecological Applications, 26, 1868–1880, https://doi.org/10.1890/15-1597.1, 2016.

Bright, R. M., Allen, M., Antón-Fernández, C., Belbo, H., Dalsgaard, L., Eisner, S., Granhus, A., Kjønaas, O. J., Søgaard, G., and Astrup, R.: Evaluating the terrestrial carbon dioxide removal potential of improved forest management and accelerated forest conversion in Norway, Global Change Biology, 26, 5087–5105, https://doi.org/10.1111/gcb.15228, 2020.

Bsaibes, A., Courault, D., Baret, F., Weiss, M., Olioso, A., Jacob, F., Hagolle, O., Marloie, O., Bertrand, N., Desfond, V., and Kzemipour, F.: Albedo and LAI estimates from FORMOSAT-2 data for crop monitoring, Remote Sensing of Environment, 113, 716–729, https://doi.org/10.1016/j.rse.2008.11.014, 2009.

Chen, A., Li, W., Li, W., and Liu, X.: An observational study of snow aging and the seasonal variation of snow albedo by using data from Col de Porte, France, Chinese Science Bulletin, 59, 4881–4889, https://doi.org/10.1007/s11434-014-0429-9, 2014.

Daudt, R. C., Wulf, H., Hafner, E. D., Bühler, Y., Schindler, K., and Wegner, J. D.: Snow depth estimation at country-scale with high spatial and temporal resolution, ISPRS Journal of Photogrammetry and Remote Sensing, 197, 105–121, https://doi.org/10.1016/j.isprsjprs.2023.01.017, 2023.

Dax, T., Schroll, K., Machold, I., Derszniak-Noirjean, M., Schuh, B., and Gaupp-Berghausen, M.: Land Abandonment in Mountain Areas of the EU: An Inevitable Side Effect of Farming Modernization and Neglected Threat to Sustainable Land Use, Land, 10, 591, https://doi.org/10.3390/land10060591, 2021.

European Environment Agency: CORINE Land Cover 2018 (raster 100 m), Europe, 6-yearly - version 2020_20u1, May 2020, https://doi.org/10.2909/960998C1-1870-4E82-8051-6485205EBBAC, 2019.

European Parliament and Council: Regulation (EU) 2018/842 of the European Parliament and of the Council of 30 May 2018, https://eur-lex.europa.eu/eli/reg/2018/842/oj, accessed: January 2, 2024, 2018.

Fernandes, R., Prevost, C., Canisius, F., Leblanc, S. G., Maloley, M., Oakes, S., Holman, K., and Knudby, A.: Monitoring snow depth change across a range of landscapes with ephemeral snowpacks using structure from motion applied to lightweight unmanned aerial vehicle videos, The Cryosphere, 12, 3535–3550, https://doi.org/10.5194/tc-12-3535-2018, 2018.

Friedl, M. and Sulla-Menashe, D.: MCD12Q1 MODIS/Terra+Aqua Land Cover Type Yearly L3 Global 500m SIN Grid V006, https://doi.org/10.5067/MODIS/MCD12Q1.006, 2019.

https://doi.org/10.5194/egusphere-2024-881
Preprint. Discussion started: 3 April 2024

GeoSphere Austria: GeoSphere Austria - Bundesanstalt für Geologie, Geophysik, Klimatologie und Meteorologie, https://www.zamg.ac.at, 2024.

Gottlieb, A. R. and Mankin, J. S.: Evidence of human influence on Northern Hemisphere snow loss, Nature, 625, 293–300, https://doi.org/10.1038/s41586-023-06794-y, 2024.

Gupta, H. V., Kling, H., Yilmaz, K. K., and Martinez, G. F.: Decomposition of the mean squared error and NSE performance criteria: Implications for improving hydrological modelling, Journal of Hydrology, 377, 80–91, https://doi.org/10.1016/j.jhydrol.2009.08.003, 2009.

Hall, D. K. and Martinec, J.: Remote Sensing of Ice and Snow, Springer Netherlands, ISBN 9789400948426, https://doi.org/10.1007/978-94-009-4842-6, 1985.

Hedrick, A., Marshall, H.-P., Winstral, A., Elder, K., Yueh, S., and Cline, D.: Independent evaluation of the SNODAS snow depth product using regional-scale lidar-derived measurements, The Cryosphere, 9, 13–23, https://doi.org/10.5194/tc-9-13-2015, 2015.

Jacob, D., Petersen, J., Eggert, B., Alias, A., Christensen, O. B., Bouwer, L. M., Braun, A., Colette, A., Déqué, M., Georgievski, G., Georgopoulou, E., Gobiet, A., Menut, L., Nikulin, G., Haensler, A., Hempelmann, N., Jones, C., Keuler, K., Kovats, S., Kröner, N., Kotlarski, S., Kriegsmann, A., Martin, E., van Meijgaard, E., Moseley, C., Pfeifer, S., Preuschmann, S., Radermacher, C., Radtke, K., Rechid, D., Rounsevell, M., Samuelsson, P., Somot, S., Soussana, J.-F., Teichmann, C., Valentini, R., Vautard, R., Weber, B., and Yiou, P.: EURO-CORDEX: new high-resolution climate change projections for European impact research, Regional Environmental Change, 14, 563–578, https://doi.org/10.1007/s10113-013-0499-2, 2013.

Jin, Y., Schaaf, C. B., Gao, F., Li, X., Strahler, A. H., Zeng, X., and Dickinson, R. E.: How does snow impact the albedo of vegetated land surfaces as analyzed with MODIS data?, Geophysical Research Letters, 29, https://doi.org/10.1029/2001gl014132, 2002.

Ke, G., Meng, Q., Finley, T., Wang, T., Chen, W., Ma, W., Ye, Q., and Liu, T.-Y.: Lightgbm: A highly efficient gradient boosting decision tree, Advances in neural information processing systems, 30, 3146–3154, https://proceedings.neurips.cc/paper_files/paper/2017/file/6449f44a102fde848669bdd9eb6b76fa-Paper.pdf, 2017.

Liu, J., Schaaf, C., Strahler, A., Jiao, Z., Shuai, Y., Zhang, Q., Roman, M., Augustine, J. A., and Dutton, E. G.: Validation of Moderate Resolution Imaging Spectroradiometer (MODIS) albedo retrieval algorithm: Dependence of albedo on solar zenith angle, Journal of Geophysical Research: Atmospheres, 114, https://doi.org/10.1029/2008jd009969, 2009.

Lugato, E., Cescatti, A., Jones, A., Ceccherini, G., and Duveiller, G.: Maximising climate mitigation potential by carbon and radiative agricultural land management with cover crops, Environmental Research Letters, 15, 94 075, https://doi.org/10.1088/1748-9326/aba137, 2020.

Matsakis, N. D. and Klock II, F. S.: The rust language, in: ACM SIGAda Ada Letters, vol. 34, pp. 103–104, ACM, 2014.

Myneni, R., Knyazikhin, Y., and Park, T.: MCD15A3H MODIS/Terra+Aqua Leaf Area Index/FPAR 4-day L4 Global 500m SIN Grid V006, https://doi.org/10.5067/MODIS/MCD15A3H.006, 2015.

NASA/METI/AIST/Japan Spacesystems And U.S./Japan ASTER Science Team: ASTER Global Digital Elevation Model V003, https://doi.org/10.5067/ASTER/ASTGTM.003, 2019.

Nash, J. and Sutcliffe, J.: River flow forecasting through conceptual models part I - A discussion of principles, Journal of Hydrology, 10, 282–290, https://doi.org/10.1016/0022-1694(70)90255-6, 1970.

Notarnicola, C.: Hotspots of snow cover changes in global mountain regions over 2000–2018, Remote Sensing of Environment, 243, 111 781, https://doi.org/10.1016/j.rse.2020.111781, 2020.

Olefs, M., Koch, R., Schöner, W., and Marke, T.: Changes in Snow Depth, Snow Cover Duration, and Potential Snowmaking Conditions in Austria, 1961–2020—A Model Based Approach, Atmosphere, 11, 1330, https://doi.org/10.3390/atmos11121330, 2020.

https://doi.org/10.5194/egusphere-2024-881
Preprint. Discussion started: 3 April 2024

Pedregosa, F., Varoquaux, G., Gramfort, A., Michel, V., Thirion, B., Grisel, O., Blondel, M., Prettenhofer, P., Weiss, R., Dubourg, V., Vanderplas, J., Passos, A., Cournapeau, D., Brucher, M., Perrot, M., and Édouard Duchesnay: Scikit-learn: Machine Learning in Python, Journal of Machine Learning Research, 12, 2825–2830, http://jmlr.org/papers/v12/pedregosa11a.html, 2011.

Potapov, P., Li, X., Hernandez-Serna, A., Tyukavina, A., Hansen, M. C., Kommareddy, A., Pickens, A., Turubanova, S., Tang, H., Silva, C. E., Armston, J., Dubayah, R., Blair, J. B., and Hofton, M.: Mapping global forest canopy height through integration of GEDI and Landsat data, Remote Sensing of Environment, 253, 112 165, https://doi.org/10.1016/j.rse.2020.112165, 2021.

Ridgwell, A., Singarayer, J. S., Hetherington, A. M., and Valdes, P. J.: Tackling Regional Climate Change By Leaf Albedo Bio-geoengineering, Current Biology, 19, 146–150, https://doi.org/10.1016/j.cub.2008.12.025, 2009.

Rouault, E., Warmerdam, F., Schwehr, K., Kiselev, A., Butler, H., Łoskot, M., Szekeres, T., Tourigny, E., Landa, M., Miara, I., Elliston, B., Chaitanya, K., Plesea, L., Morissette, D., Jolma, A., and Dawson, N.: GDAL, https://doi.org/10.5281/zenodo.5884351, 2023.

Ryu, Y., Jiang, C., Kobayashi, H., and Detto, M.: MODIS-derived global land products of shortwave radiation and diffuse and total photosynthetically active radiation at 5 km resolution from 2000, Remote Sensing of Environment, 204, 812–825, https://doi.org/10.1016/j.rse.2017.09.021, 2018.

Sagan, C., Toon, O. B., and Pollack, J. B.: Anthropogenic Albedo Changes and the Earth's Climate, Science, 206, 1363–1368, https://doi.org/10.1126/science.206.4425.1363, 1979.

Schaaf, C. and Wang, Z.: MCD43A1 MODIS/Terra+Aqua BRDF/Albedo Model Parameters Daily L3 Global - 500m V006, https://doi.org/10.5067/MODIS/MCD43A1.006, 2015.

Stephens, G. L., O'Brien, D., Webster, P. J., Pilewski, P., Kato, S., and Li, J.: The albedo of Earth, Reviews of Geophysics, 53, 141–163, https://doi.org/10.1002/2014rg000449, 2015.

The Geoportal of the nine Austrian Provinces: Digital Terrain Model of Austria, based on Airborne Laserscanning, https://www.geoland.at, 2024.

Umweltbundesamt GmbH: Austrias Annual Greenhouse Gas Inventory 1990-2021, Umweltbundesamt GmbH, Vienna, Austria, ISBN 978-3-99004-670-8, https://www.umweltbundesamt.at/, 2023.

Van Rossum, G. and Drake, F. L.: Python 3 Reference Manual, CreateSpace, Scotts Valley, CA, ISBN 1441412697, 2009.

Webster, C. and Jonas, T.: Influence of canopy shading and snow coverage on effective albedo in a snow-dominated evergreen needleleaf forest, Remote Sensing of Environment, 214, 48–58, https://doi.org/10.1016/j.rse.2018.05.023, 2018.

Wiscombe, W. J. and Warren, S. G.: A Model for the Spectral Albedo of Snow. I: Pure Snow, Journal of the Atmospheric Sciences, 37, 2712–2733, https://doi.org/10.1175/1520-0469(1980)037<2712:amftsa>2.0.co;2, 1980.

Wohlfahrt, G., Tomelleri, E., and Hammerle, A.: The albedo–climate penalty of hydropower reservoirs, Nature Energy, 6, 372–377, https://doi.org/10.1038/s41560-021-00784-y, 2021.

Yin, T., Zhai, Y., Zhang, Y., Yang, W., Dong, J., Liu, X., Fan, P., You, C., Yu, L., Gao, Q., Wang, H., Zheng, P., and Wang, R.: Impacts of climate change and human activities on vegetation coverage variation in mountainous and hilly areas in Central South of Shandong Province based on tree-ring, Frontiers in Plant Science, 14, https://doi.org/10.3389/fpls.2023.1158221, 2023.